Unveiling the ionic exchange mechanisms in vertically-oriented graphene nanosheet supercapacitor electrodes with electrochemical quartz crystal microbalance and ac -electrogravimetry

Tao Le, David Aradilla, Gérard Bidan, Florence Billon, Marc Delaunay, Jean-Michel Gérard, Hubert Perrot, Ozlem Sel

Unveiling the ionic exchange mechanisms in vertically-oriented graphene nanosheet supercapacitor electrodes with electrochemical quartz crystal microbalance and *ac*-electrogravimetry

T. Lé[a,c], D. Aradilla[a,*], G. Bidan[a], F. Billon[c], M. Delaunay[b], J.M. Gérard[b], H. Perrot[c] and O. Sel[c,*]

[a]*Univ. Grenoble Alpes, CEA, CNRS, INAC-SyMMES, F-38000 Grenoble, France*

[b]*Univ. Grenoble Alpes, CEA, INAC-PhELIQS, F-38000 Grenoble, France*

[c] *Sorbonne Université, CNRS, Laboratoire Interfaces et Systèmes Électrochimiques, LISE, 75005 Paris, France*

*Corresponding authors: Ozlem.sel@upmc.fr and David.ARADILLA@cea.fr

Abstract

This work presents the first electrochemical quartz crystal microbalance (EQCM) results for vertically-oriented graphene nanosheets (VOGNs) as supercapacitor electrodes. Conventional EQCM technique delivered primary insights on the ionic exchange mechanisms between VOGNs and organic electrolytes, showing a major contribution of anions. A more advanced electrogravimetric methodology, *ac*-electrogravimetry, was then used to access specific dynamic attributes for each species exchanged at the VOGN electrode surface. Accordingly, under the conditions of this study, anions were confirmed to be the major energy storage vector with high kinetic values and low transfer resistance while cations and free solvent molecules are given non-negligible supporting roles.

Keywords: Supercapacitors, Microbalance, *ac*-electrogravimetry, Graphene

1. Introduction

The stunning capabilities of supercapacitor devices in terms of power density and cycling stability has led many research groups to focus on nanostructured carbonaceous materials with enhanced capacitance and lifetime performances [1]. Among such materials, VOGNs have recently shown a great potential as electrodes for electrochemical double layer capacitors (EDLCs) due to their peculiar characteristics such as high conductivity, ion access facility and open structure with high surface area [2-4]. In spite of the numerous conventional morphological, structural and physical-chemical techniques employed for their characterization, a better understanding of the electrochemical processes involved in VOGN electrodes has not yet been provided with in-situ characterization techniques. In this direction, EQCM is commonly used to complement the electrochemical analysis with in situ gravimetric measurements, unraveling new insights on the ionic transfer mechanisms occurring at the electrode-electrolyte interface [5, 6]. Mass and charge variations measured simultaneously during the electrode cycling allow the derivation of the global mass per mole of electrons (MPE) that is exchanged between the electrode and the electrolyte according to the following equation [7, 8]:

$$MPE = F\frac{\Delta m}{\Delta q} = F\frac{\Delta m/\Delta t}{\Delta q/\Delta t} \quad \text{(eq. 1)}$$

with F the Faraday number, Δm and Δq the mass and charge variations respectively.

The average mass and charge variations measured with classical EQCM give a general understanding of the exchange processes, but only few details on the dynamic behaviour of individual ions or solvent molecules. This study aims at overcoming these limitations with *ac*-electrogravimetry, a non-conventional technique combining the mass measurements with electrochemical impedance spectroscopy (EIS) to deconvolute the classical EQCM response.

Frequency dependant mass and charge variations are obtained under a fixed potential with a small sinusoidal perturbation and used to generate both the classical EIS transfer function (TF) $\frac{\Delta E}{\Delta I}$ and the mass/potential TF $\frac{\Delta m}{\Delta E}$. These TF are then fitted with an appropriate model to obtain detailed identification of the species involved in the charge transfer mechanism, along with the kinetics and the concentrations associated with each species [8-12]. We here report the results from both classical EQCM and its complementary counterpart *ac*-electrogravimetry on VOGN electrodes directly grown on the microbalance device.

2. Experimental

2.1 Materials and reagents

Anhydrous propylene carbonate (PC) and tetrabutylammonium tetrafluoroborate ($TBABF_4$) were purchased from Sigma Aldrich and used without further purification. $GaPO_4$ plain crystals with a diameter of 14 mm were purchased from AWS company (Spain).

2.2 Synthesis of VOGNs on $GaPO_4$ microbalance

VOGNs were synthesized by electron cyclotron resonance-chemical vapor deposition (ECR-CVD) through a reactor built in CEA-Grenoble [13]. The experimental conditions have been reported in our previous works [14, 15]. Thus, briefly, VOGNs were grown on $GaPO_4$ substrates at a temperature of 480°C during 80 min at $2 \cdot 10^{-3}$ mbar, (7 µg deposited).

2.3 Morphological characterization of the electrodes

The morphology of the VOGNs was examined by using a ZEISS Ultra 55 SEM operating at an accelerating voltage of 10 kV.

2.4 Electrogravimetric characterization with EQCM and ac-electrogravimetry

A lab-made QCM device (Miller oscillator) was used to measure Δf of the $GaPO_4$ crystal (~6 MHz) which is then converted into mass changes using the Sauerbrey equation: $\Delta f = -k_s \cdot \frac{\Delta m}{A}$ where A is the electrode surface and k_s is the sensitivity factor (Theoretical value: $7.92 \cdot 10^7\ Hz\ g^{-1}\ cm^2$) [16]. A solution of PC containing 0.5 M $TBABF_4$ was used as electrolyte, with a platinum grid as counter electrode and acetonitrile-based Ag/Ag^+ reference electrode. This EQCM setup was used to perform cyclic voltammetry (CV) combined with mass variation measurements in a potential window from -1.5 V to 1V vs Ag/Ag^+ at scan rates from 10 to 100 mV s^{-1}. An open-circuit-potential of 175 mV vs Ag/Ag^+ was measured. *Ac*-electrogravimetry was then performed for 11 potentials ranging from -1.5 V to 1V vs Ag/Ag^+ using a frequency response analyzer (Solartron-1254) and a lab-made potentiostat (SOTELEM-PGSTAT). For each potential, the electrode was polarized and a potential perturbation (80 mV) was superimposed (relatively high perturbation was necessary to obtain measurable mass variations in *ac*-electrogravimetry while keeping a linear response).

.

The mass change Δm of the working electrode was measured simultaneously with the *ac* response, ΔI, of the electrochemical system. The frequency range was between 63 kHz and 10 mHz. The four-channel FRA was then used to obtain the electrogravimetric transfer function, $\frac{\Delta m}{\Delta E}(\omega)$, and the electrochemical impedance, $\frac{\Delta E}{\Delta I}(\omega)$ simultaneously at a given potential [8].

3. Results and discussion

Figure 1a shows the morphology of VOGNs grown by ECR-CVD on gold-coated $GaPO_4$ crystals (inset). According to the SEM image, VOGNs s are organized in a dense layer of graphene sheets that grow perpendicular to the substrate's surface, which was found in excellent agreement with our previous works using SEM, TEM and Raman spectroscopy [14, 15]. A thickness of 1 µm was estimated by a cross-sectional view.

Figure 1b depicts the CV and the mass variations measured simultaneously (EQCM) on the electrode before and after the VOGN growth at a scan rate of 100 mV s^{-1}. The CV response on VOGNs displays a good capacitive behavior according to our previous works [14, 15]. Nevertheless, an increase of the current density from 0.2 V was ascribed to chemical reactions of gold and the peak at 0 V was associated to impurities in the electrolyte or the presence of oxygen groups on VOGNs [17]. These reactions have a contribution to the mass variations below 30 ng while the mass of the electrode with VOGNs increases by ~200 ng between -1 V and 1 V and decreases by the same amount during the reverse scan, showing completely reversible mass intakes when the electrode is positively charged. Such behaviour is associated with anion electro-adsorption at the electrode surface. A slight reversible mass increase is also measured during the reverse scan between -1 V and -1.5 V. This is associated with cation electro-adsorption on the negatively charged electrode. The same measurements at scan rates from 10 to 50 mV s^{-1} gave similar results. Figure 1c depicts the MPE calculated using eq. 1 for all potentials where the current is not near zero. Positive and negative values of the MPE correspond to a major contribution to the energy storage mechanism by anions and cations, respectively. If only one species is exchanged, then the MPE corresponds to its molar mass. Here, we obtain a MPE of ~80 and ~50 g.mol^{-1} above 0 V for decreasing and increasing potentials, respectively. For decreasing potentials, it is close to the BF_4^- ion's molar mass (86 g.mol^{-1}), indicating almost solely anion exchange. This value lowers at the increasing potentials (~50 g.mol^{-1}), indicating complex interfacial behavior. Below 0 V the MPE values decrease, suggesting that multiple species are exchanged [18]. In such cases, using Faradays' law to interpret classical EQCM data reaches its limitations. To discriminate between the involved species, Donnan-type electrical double layer models were used [19]. However, kinetic analysis of ion electroadsorption/(desorption) by classical EQCM remains limited to scan rates of the CV.

To overcome these limitations, complementary *ac*-electrogravimetric measurements were necessary. The squares and circles on Figure 2a (resp. 2b) depict the Nyquist plot of the resulting experimental charge/potential TF $\frac{\Delta q}{\Delta E}(\omega)$ and mass/potential TF $\frac{\Delta m}{\Delta E}(\omega)$ at two potentials, 1 V and -1 V. The mass/potential TF ($\frac{\Delta m}{\Delta E}(\omega)$) obtained at all potentials shows a clear suppressed loop in the first quadrant at frequencies ranging from 0.01 Hz to 10 Hz. It is characteristic for anion contribution in *ac*-electrogravimetry.

The experimental data were fitted with a model described in previous works [9-12] in a configuration where the electrolyte's cations (TBA^+), anions (BF_4^-) and free solvent molecules (PC) are exchanged. Within this model, the theoretical TFs for $\frac{\Delta q}{\Delta E}(\omega)$ and $\frac{\Delta m}{\Delta E}(\omega)$ are calculated using eq. 2 and 3 and depicted as continuous lines in Figure 2:

$$\frac{\Delta q}{\Delta E}(\omega) = \mathrm{F} \cdot \mathrm{d}\left(\frac{\mathrm{G_a}}{\mathrm{j}\omega d + K_a} - \frac{\mathrm{G}_c}{\mathrm{j}\omega d + K_c}\right) \quad \text{(eq. 2)}$$

$$\frac{\Delta m}{\Delta E}(\omega) = -\mathrm{d}\left(\mathrm{m_a}\frac{\mathrm{G_a}}{\mathrm{j}\omega d + K_a} + \mathrm{m_c}\frac{\mathrm{G}_c}{\mathrm{j}\omega d + K_c} + \mathrm{m_s}\frac{\mathrm{G_s}}{\mathrm{j}\omega d + K_s}\right) \qquad \text{(eq. 3)}$$

where K_i is the kinetic parameter and G_i is the parameters related to the ease of interfacial transfer for each species (*i=a (anion), c (cation), s (solvent)*), $\omega = 2\pi f$ and d the film thickness.

For potentials above 0.25 V, cations, anions and free solvent molecules are required in the model to obtain a perfect match for both the TFs $\frac{\Delta q}{\Delta E}(\omega)$ and $\frac{\Delta m}{\Delta E}(\omega)$. For potentials between -0.25 V and 0.25 V, no cation contribution was needed to fit the TFs and it was thus removed from the model. For potentials below -0.25 V free solvent molecules are not required to fit the TFs, therefore a configuration with only cations and anions was used. Using eq. 3, the partial mass/potential TFs were calculated by removing the contribution of anions (resp. cations) to $\frac{\Delta m}{\Delta E}(\omega)$ and their Nyquist plots were depicted in Figure 2c (resp. Figure 2d). At 1 V vs Ag/Ag$^+$, the cation-solvent partial mass/potential TF (Figure 2c) shows a loop in the third quadrant for frequencies above 0.1 Hz, characteristic for cation contribution. Below 0.1 Hz this loop continues towards the upper quadrants as a result of free solvent molecules being exchanged with the same flux direction as the anions. At -1 V the solvent's contribution disappears and only the cation contribution can be seen. The anion-solvent partial mass/potential TF (Figure 2d) displays suppressed loops in the 1st quadrant (characteristic for anion contribution) with a diameter around 5 times greater than those from the $\frac{\Delta m}{\Delta E}(\omega)$ TF (Figure 2b) for which the loops were diminished by the cation contribution. Figure 2e depicts the evolution of the kinetic parameters K_i obtained for each species in the model at all the studied potentials. Anions always have slightly higher kinetic parameters (K_a = 4·10^{-4} to 1.2·10^{-3} cm s^{-1}) than cations (K_c = 3·10^{-4} to 8.5·10^{-4} cm s^{-1}), showing a faster ionic transfer of the BF_4^- compared to the heavier TBA$^+$ (M_{TBA+} = 242.46 g mol$^-$

^{1}). Free solvent molecules are exchanged above -0.5 V but at very slow rates of transfer (K_s = $2\cdot10^{-6}$ to $5\cdot10^{-6}$ cm s^{-1}). The parameters G_i of each species are used to calculate the transfer resistance, $Rt_i = \frac{1}{FG_i}$, depicted in Figure 2f at all the studied potentials. Free solvent molecules have the highest transfer resistance (Rt_s = 17 to 38 kΩ cm^2), followed by cations (Rt_c = 0.4 to 6 kΩ cm^2) while anions have the lowest transfer resistance (Rt_a = 100 to 150 Ω cm^2).

The values of K_i and G_i collected for each species at various potentials revealed the dynamics of the charge transfer mechanism, showing that BF_4^- anions have a major contribution to the energy stored in VOGN electrodes under the conditions of this study. These values also allow the calculation of the relative concentration changes of individual species C_i-C_0 to be done. For that, an integration of $\left.\frac{\Delta C_i}{\Delta E}\right|_{\omega\to 0} = -\frac{G_i}{K_i}$ is realized following the same procedure as given in references [9-11]. Figure 3a depicts C_i-C_0 calculated for each species, showing that BF_4^- anions have the largest concentration variations which increase linearly from -1.5 V to 1 V vs Ag/Ag^+. Free solvent molecules follow the same concentration variations as the anions between -0.5 V and 1 V while the concentration of cations rises very slightly at negative potentials (-0.75 V to -1.5 V vs Ag/Ag+). These results show that BF_4^- anions are the main species that contribute to the energy storage mechanism in this configuration, with a perm-selectivity failure between -1.5V to -0.5 V.

The concentration variations C_i-C_0 can be turned into mass variations m_i for each species in the volume of the porous VOGN electrode $V_{electrode}$ ($m_i = M_i \cdot V_{electrode} \cdot (C_i - C_0)$ with M_i the molar mass of species *i*). Figure 3b depicts the total mass variations measured in CV and calculated with $m = \sum m_i$, with the individual calculated mass variations m_i depicted in the inset. Δm calculated from *ac*-electrogravimetry is in good agreement with the Δm given by our classical EQCM. This indicates the utility of *ac*-electrogravimetry to deconvolute the EQCM response into individual contributions. This was also possible by using advanced global EQCM analysis [20].

Conclusions

The energy storage mechanisms in VOGN supercapacitor electrodes were deeply investigated for the first time using EQCM and *ac*-electrogravimetry method. After achieving a successful growth of VOGNs on piezoelectric $GaPO_4$ resonators, EQCM measurements in an organic electrolyte of PC containing 0.5M $TBABF_4$ led to first insights on the charge transfer mechanism, showing that anion electro-adsorption played a major role. This evidence was further proved and scrutinized by *ac*-electrogravimetry which enabled the deconvolution of the global EQCM outcome into individual dynamic responses for each species exchanged at the electrode/electrolyte interface. BF_4^- anions were found to be faster than their cation counterpart, and to have the highest concentration variations along the whole electrochemical window.

Acknowledgements

This work was supported by the ANR-11-IDEX-0004-02 and the Cluster of Excellence-LABEX-MATISSE-Sorbonne Université. T. Lé acknowledges also CEA for financial support.

References

[1] A. Tyagi, K.M. Tripathi, R.K. Gupta, Recent progress in micro-scale energy storage devices and future aspects, J. Mater. Chem. A. 3 (2015) 22507–22541.

[2] Z. Bo, S. Mao, Z.J. Han, K. Cen, J. Chen, K.K. Ostrikov, Emerging energy and environmental applications of vertically-oriented graphenes, Chem. Soc. Rev. 44 (2015) 2108–2121.

[3] G. Xiong, C. Meng, R. G. Reifenberger, P. P. Irazoqui, T. S. Fisher, A review of graphene-based electrochemical microsupercapacitors, Electroanalysis. 26 (2014) 30 - 51.

[4] C. Junhong, Z. Bo, L. Ganhua, Vertically-oriented Graphene: PECVD Synthesis and Applications, Chapter 7: Vertically-oriented graphene supercapacitors, Ed. Springer, 2015, pp. 79-94.

[5] S. Sigalov, M.D. Levi, G. Salitra, D. Aurbach, J. Maier, EQCM as a unique tool for determination of ionic fluxes in microporous carbons as a function of surface charge distribution, Electrochem. Commun. 12 (2010) 1718–1721.

[6] W. Tsai, P. Taberna, P. Simon, Electrochemical Quartz Crystal Microbalance (EQCM) Study of Ion Dynamics in Nanoporous Carbons, J. Am. Chem. Soc. 136 (2014) 8722–8728.

[7] F. Escobar-Teran, A. Arnau, J. Garcia, Y. Jiménez, H. Perrot, O. Sel, Gravimetric and dynamic deconvolution of global EQCM response of carbon nanotube based electrodes by Ac-electrogravimetry, Electrochem. Commun. 70 (2016) 73–77.

[8] H. Goubaa, F. Escobar-Teran, I. Ressam, W. Gao, A.E. Kadib, I.T. Lucas, M. Raihane, M.

Lahcini, H. Perrot, O. Sel, Dynamic Resolution of Ion Transfer in Electrochemically Reduced Graphene Oxides Revealed by Electrogravimetric Impedance, J. Phys. Chem. C. 121 (2017) 9370–9380.

[9] C. Gabrielli, J.J. García-Jareño, M. Keddam, H. Perrot, F. Vicente, Ac-Electrogravimetry Study of Electroactive Thin Films. I. Application to Prussian Blue, J. Phys. Chem. B. 106 (2002) 3182–3191.

[10] C. Gabrielli, M. Keddam, N. Nadi, H. Perrot, Ions and solvent transport across conducting polymers investigated by ac electrogravimetry. Application to polyaniline, J. Electroanal. Chem. 485 (2000) 101–113.

[11] L.T. Kim, C. Debiemme-Chouvy, C. Gabrielli, H. Perrot, Redox Switching of Heteropolyanions Entrapped in Polypyrrole Films Investigated by ac Electrogravimetry, Langmuir. 28 (2012) 13746–13757.

[12] D. Benito, C. Gabrielli, J. García-Jareño, M. Keddam, H. Perrot, F. Vicente, An electrochemical impedance and ac-electrogravimetry study of PNR films in aqueous salt media, Electrochem. Commun. 4 (2002) 613–619.

[13] M. Delaunay, M.N. Semeria, Method and device for electronic cyclotronic resonance plasma deposit of carbon nanofibre layers in fabric form and resulting fabric layers, (2004). https://www.google.fr/patents/US6787200.

[14] D. Aradilla, M. Delaunay, S. Sadki, J.M. Gérard, G. Bidan, Vertically aligned graphene nanosheets on silicon using an ionic liquid electrolyte: towards high performance on-chip micro-supercapacitors, J. Mater. Chem. A. 3 (2015) 19254–19262.

[15] D. Aradilla, M. Delaunay, M. Buhagiar, D. Aldakov, J. Faure-Vincent, H. Okuno, J.M.

Gérard, G. Bidan, Plasma Heavily Nitrogen-Doped Vertically Oriented Graphene Nanosheets (N-VOGNs) for High Volumetric Performance On-Chip Supercapacitors in Ionic Liquid, Curr. Smart Mater. 2 (2017) 1–8.

[16] S. Jakab, S. Picart, B. Tribollet, P. Rousseau, H. Perrot, C. Gabrielli, Study of the Dissolution of Thin Films of Cerium Oxide by Using a $GaPO_4$ Crystal Microbalance, Anal. Chem. 81 (2009) 5139–5145.

[17] S. Ghosh, T. Mathews, B. Gupta, A. Das, G. N. Krishna, M. Kamruddin, Supercapacitive vertical graphene nanosheets in aqueous electrolytes, Nano-Structures & Nano-Objects. 10 (2017) 42–50.

[18] C. R. Arias, C. Debiemme-Chouvy, C. Gabrielli, C. Laberty-Robert, A. Pailleret, H. Perrot, O. Sel, New Insights into Pseudocapacitive Charge-Storage Mechanisms in Li-Birnessite Type MnO2 Monitored by Fast Quartz Crystal Microbalance Methods, J. Phys. Chem. C 118 (2014), 26551-26559.

[19] N. Shpigel, M. D. Levi, S. Sigalov, D. Aurbach, L. Daikhin, V. Presser, Novel in situ multiharmonic EQCM-D approach to characterize complex carbon pore architectures for capacitive deionization of brackish water, J. Phys. Condens. Matter 28 (2016) 114001.

[20] S. Sigalov, M. D. Levi, G. Salitra, D. Aurbach, A. Jänes, E. Lust, I. C. Halalay, Selective adsorption of multivalent ions into TiC-derived nanoporous carbon, Carbon 50 (2012) 3943-3960.

Figure Captions

Figure 1. a) SEM image of VOGNs grown on gold-patterned $GaPO_4$ electrode (full electrode pictured in inset), b) cyclic voltammetry coupled with the mass measurement of the electrode before growth (Au) and after growth (VOGNs) at 100 mV s^{-1} and c) MPE calculated at all potentials with non-negligible current density.

Figure 2. a-d) Nyquist plots of the experimental and theoretical results of *ac*-electrogravimetry on VOGN electrodes at 1V and -1V, depicting a) the charge/potential TFs $\frac{\Delta q}{\Delta E}(\omega)$, b) the mass/potential TFs $\frac{\Delta m}{\Delta E}(\omega)$, c) the cation-solvent partial mass/potential TFs and d) the anion-solvent partial mass/potential TFs. e) Evolution of the kinetic parameters K_i (cm s^{-1}) and f) Evolution of the transfer resistance values Rt_i (Ω cm^2).

Figure 3. a) Evolution of the relative concentrations, $C_i - C_0$, of each species exchanged, derived from *ac*-electrogravimetric measurements. b) Total mass variations from EQCM (blue line) calculated from *ac*-electrogravimetry results for individual species (inset) and summed (purple dotted line) as a function of the potential.

Figure 1:

a)

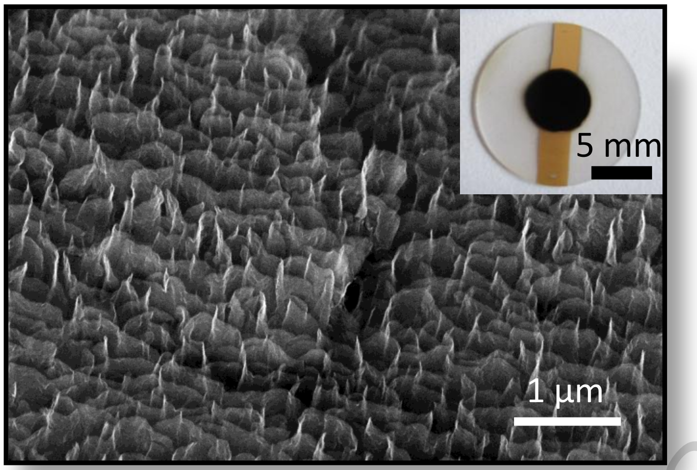
5 mm
1 µm

b)

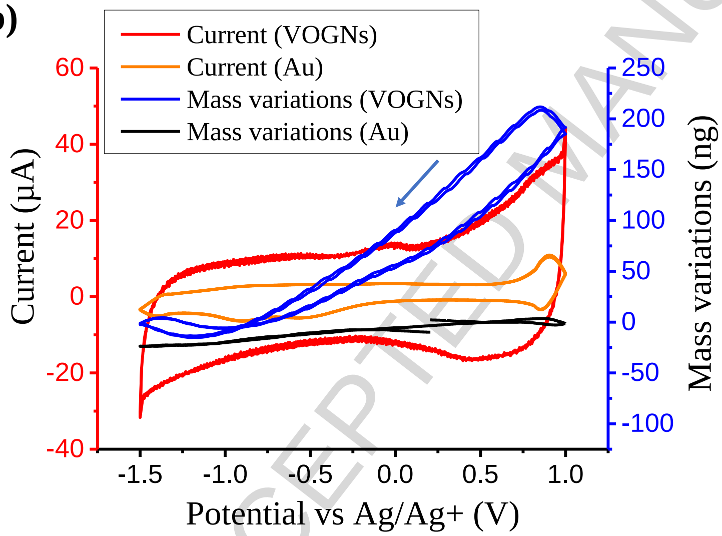
Current (VOGNs)
Current (Au)
Mass variations (VOGNs)
Mass variations (Au)
Current (µA)
Mass variations (ng)
Potential vs Ag/Ag+ (V)
60
40
20
0
-20
-40
250
200
150
100
50
0
-50
-100
-1.5
-1.0
-0.5
0.0
0.5
1.0

c)

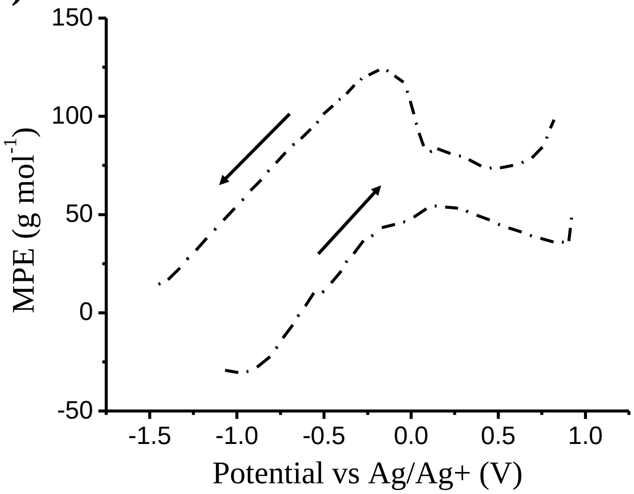

Figure 2:

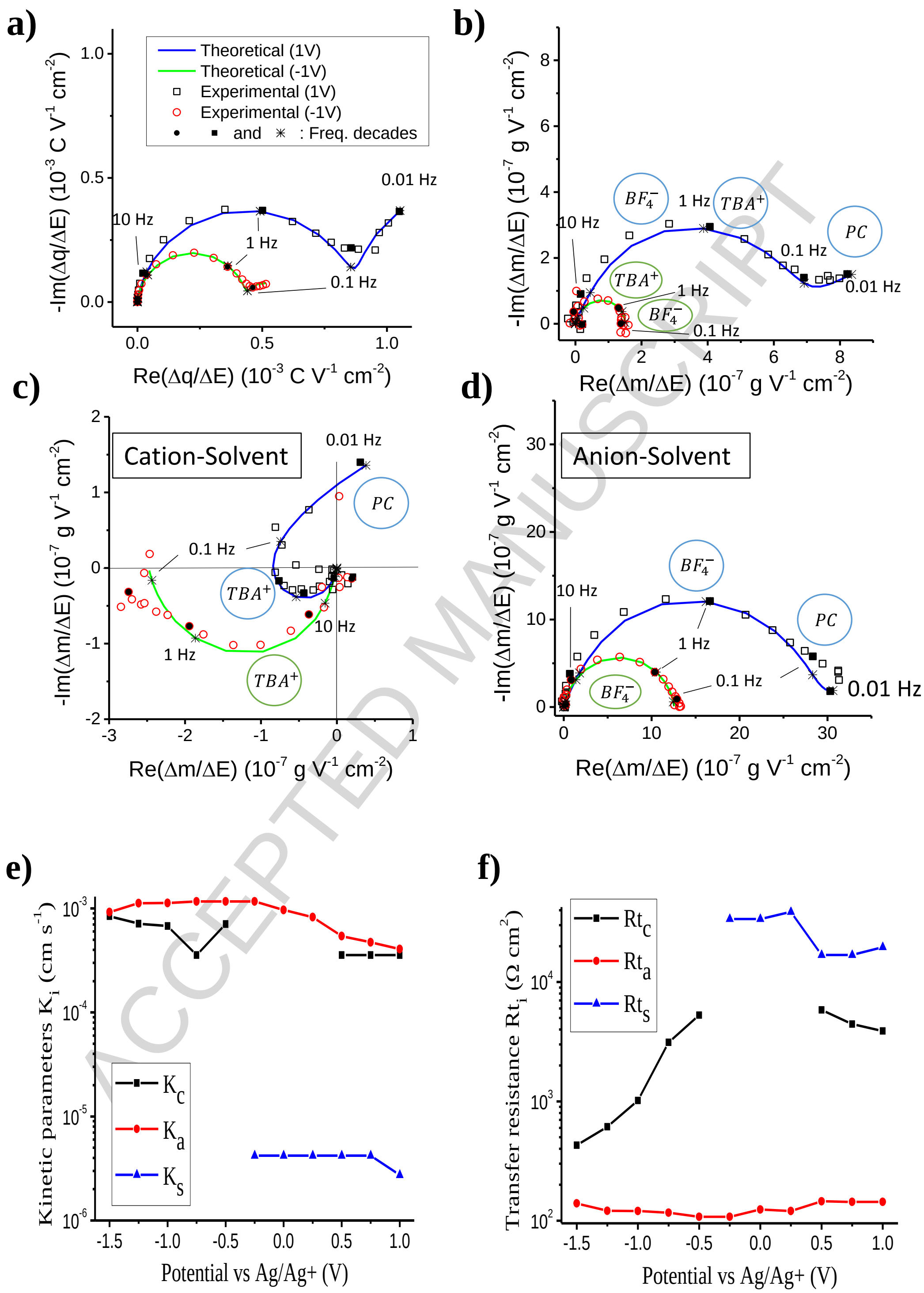
a)
Theoretical (1V)
Theoretical (-1V)
Experimental (1V)
Experimental (-1V)
and : Freq. decades
10 Hz
1 Hz
0.1 Hz
0.01 Hz
-Im(Δq/ΔE) (10^-3 C V^-1 cm^-2)
Re(Δq/ΔE) (10^-3 C V^-1 cm^-2)
b)
10 Hz
1 Hz
0.1 Hz
0.01 Hz
PC
-Im(Δm/ΔE) (10^-7 g V^-1 cm^-2)
Re(Δm/ΔE) (10^-7 g V^-1 cm^-2)
c)
Cation-Solvent
0.01 Hz
0.1 Hz
10 Hz
1 Hz
PC
-Im(Δm/ΔE) (10^-7 g V^-1 cm^-2)
Re(Δm/ΔE) (10^-7 g V^-1 cm^-2)
d)
Anion-Solvent
10 Hz
1 Hz
0.1 Hz
0.01 Hz
PC
-Im(Δm/ΔE) (10^-7 g V^-1 cm^-2)
Re(Δm/ΔE) (10^-7 g V^-1 cm^-2)
e)
Kinetic parameters K_i (cm s^-1)
Potential vs Ag/Ag+ (V)
f)
Transfer resistance Rt_i (Ω cm^2)
Potential vs Ag/Ag+ (V)

Figure 3:

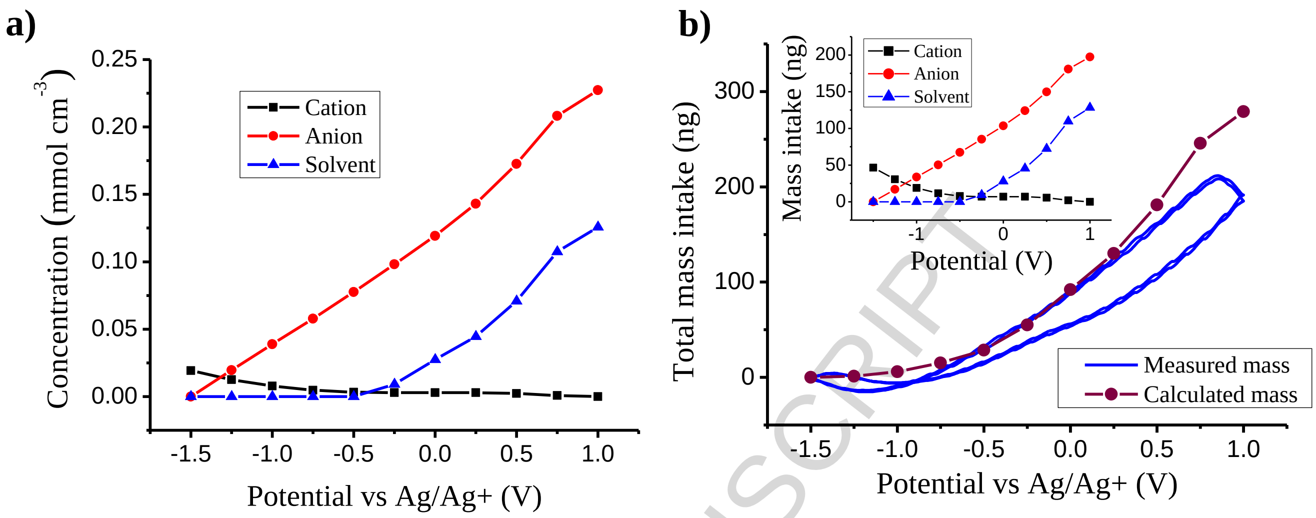
a)
Concentration (mmol cm^{-3})
0.25
0.20
0.15
0.10
0.05
0.00
Cation
Anion
Solvent
-1.5
-1.0
-0.5
0.0
0.5
1.0
Potential vs Ag/Ag+ (V)
b)
Total mass intake (ng)
300
200
100
0
Mass intake (ng)
200
150
100
50
0
Cation
Anion
Solvent
-1
0
1
Potential (V)
Measured mass
Calculated mass
-1.5
-1.0
-0.5
0.0
0.5
1.0
Potential vs Ag/Ag+ (V)

Graphical Abstract

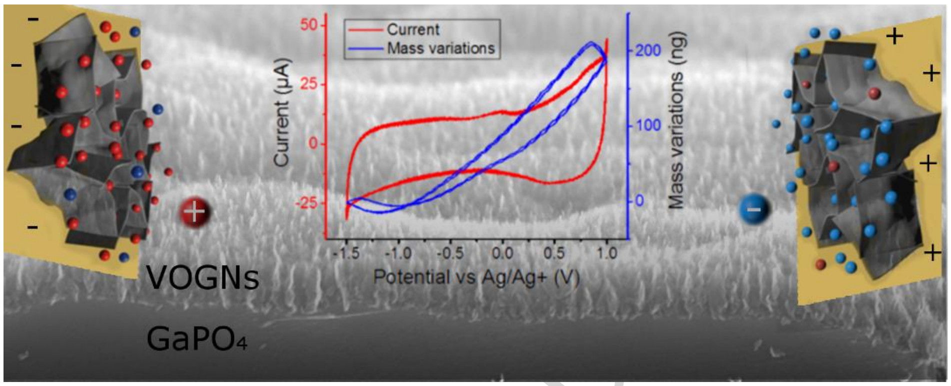

Highlights

- The mass of ions at the graphene surface is precisely measured in a varying potential
- BF_4^- anions exhibit a higher mobility than cations and are the main exchanged species
- Cyclic voltammetry mass variations were reconstructed using ac-Electrogravimetry